This document contains the draft version of the following paper:

W. Bejgerowski, A. Ananthanarayanan, D. Mueller and S.K. Gupta, "Integrated product and process design for a flapping wing drive-mechanism," *ASME Journal of Mechanical Design*, 131 (6): 061006, 2009.

Readers are encouraged to get the official version from the journal's website or by contacting Dr. S.K. Gupta (skgupta@umd.edu).

Integrated Product and Process Design for a Flapping Wing Drive-Mechanism

Wojciech Bejgerowski, Arvind Ananthanarayanan, Dominik Mueller and Satyandra K. Gupta[1]*

Department of Mechanical Engineering, University of Maryland, College Park, MD 20742
*Institute for Systems Research, University of Maryland, College Park, MD 20742

Abstract

Successful realization of a flapping wing micro air vehicle (MAV) requires development of a light weight drive-mechanism that can convert the continuous rotary motion of the motor into oscillatory flapping motion of the wings. The drive mechanism should have low weight to maximize the payload and battery capacity. It should also have high power transmission efficiency to maximize the operational range and minimize weight of the motor. In order to make flapping wing MAVs attractive in search, rescue, and recovery efforts, they should be disposable from the cost point of view. Injection molded compliant drive-mechanisms are an attractive design option because of manufacturing scalability and reduction in the number of parts. However, realizing compliant drive mechanism using injection molding requires use of multi-piece multi-gate molds. Molding process constraints need to be considered during the design stage to successfully realize the drive mechanism. This paper describes an approach for determining the drive mechanism shape and size that meets both the design and molding requirements. The novel aspects of this work include (1) minimizing the number of mold pieces and (2) the use of sacrificial shape elements to reduce the impact of the weld-lines on the structural performance. The design generated by the approach described in this paper was utilized to realize an operational flapping wing MAV.

1 Introduction

Flapping wing micro air vehicles (MAVs) are expected to present several advantages over conventional MAVs [1-8]. Birds and insects are well known for their high degree of maneuverability and quiet flights. Hence, flapping wing MAVs are also expected to be quiet because of low frequency operation, which is suitable for surveillance applications. Flapping wing MAVs can also fly at very low forward speed, making them well suited for obstacle avoidance in indoor operations.

Several researchers have developed mechanisms to realize the flapping motion and used these mechanisms in MAVs to demonstrate a flapping-wing flight. The main emphasis in these works is on the wing design and the kinematics of the mechanism. We will review representative works in this area in the following paragraphs.

Madangopal et al. [1, 2] developed and characterized a flapping wing mechanism inspired by insect and bird flight study. They presented the kinematic model and the rigid-body dynamic model of the mechanism and proposed an aerodynamic model of the wings' motion. They have also optimized the energy required to drive the system by introduction of tension springs. They reported a successful flight of the MAV prototype.

Galinski and Zbikowski [3] explored the material challenges in the design of a wing in a flapping wing mechanism, based on the insect hovering kinematics. They used two coupled four-bar linkage mechanisms to generate figure-of-eight motion. They predicted aerodynamic loading on the wing and presented an approach for the wing and mechanism design and manufacturing. They concentrated on a robust test rig design rather then a lightweight mechanism optimized for flight due to aerodynamic uncertainties and the need of laboratory testing.

Cox et al. [4] described piezoelectrically actuated flexure-based skeletal mechanisms and wings for the electromechanical emulation of mesoscale flapping flight. Authors argue that the elastodynamic properties of compliant mechanisms can be exploited for enhanced operating characteristics and lead to simple, small-scale mechanisms. They developed and tested two four-bar and one five-bar linkage designs. They proposed a wing design with a passive dynamic behavior to obtain a relative phase between wing translation and rotation and maximized its efficiency. However, they did not present any successful flight test results.

[1] Corresponding Author

Banala and Agrawal [5] developed a compound mechanism consisting of a five-bar and a four-bar linkage to mimic an insect wing motion, figure-of-eight motion. This pattern includes out-of-stroke plane motion and time varying twist in the wing. As part of their work, they optimized the wing-tip paths and twists for three different speeds using hawk moth kinematic flight data. The mechanism prototype was manufactured and tested.

Conn et al. [6] presented a biomimetic analysis of an insect flight and proposed biomimetic guidelines for mechanism simplification. Authors classified several MAV drive mechanisms by the level of constraint they impose. A novel parallel crank-rocker MAV flapping mechanism was chosen to replicate insect wing kinematics. This mechanism has an integrated flapping and pitching, not constrained output motion, which allows the adjustment of the wing angle of attack and promises the stability and maneuverability of the MAV. The prototype was manufactured and aerodynamic tests were performed.

Tantanawat and Kota [7] have described a methodology for minimizing input power in dynamics applications using both rigid body as well compliant mechanisms. As a part of their work, they analyze power consumption of a four-bar flapping mechanism. They show that the stored elastic energy can be used to reduce the power requirements for the mechanism. However, as part of their work, they did not present a detailed design.

Zdunich et al. [8] developed and tested the Mentor flapping wing MAV. They described the experimental development of the wing design and its unsteady-airfoil analysis. Authors report that due to scaling and power limitations, use of the brushless DC motors is more efficient than electroactive polymer artificial muscles. They present two successfully flying prototypes and analyze the flight tests results, incorporating them into an onboard control system stabilizing the flight.

Existing work does not fully address the challenges envisaged during the field deployment of flapping wing MAVs. Successful development of such MAVs requires further fundamental advances in the following areas:

- ***Reduction in Drive Mechanism Weight***: Current flapping wing MAV designs have very limited payload capabilities. This seriously limits the number of on-board sensors and the flight time. A main contributor to the weight controlled by the designer is the drive mechanism that converts motor's rotary motion into the flapping motion of the wings. We decided to use polymer as the material to reduce the weight of the drive mechanism. This will allow for MAVs to carry more auxiliaries. Reduction in the weight will also enable the use of larger and more powerful electronics and hence increase the payload carrying capability and the overall mission time. However, we have to ensure that the reduction in weight will not compromise the structural strength of the mechanism under operation loads. By performing detailed analysis of various forces acting on the structure, we will be able to optimize the shape of the drive mechanism to minimize the weight and retain structural strength.

- ***Low Cost***: Currently, experimental flapping wing MAV platforms are mainly produced by CNC machining. This leads to two issues: 1) CNC machining is not a scalable process and is not feasible for low cost production of MAVs and 2) Restrictions on part fabrication capabilities on 3-axis CNC machines leads to increase in part count. This leads to increased assembly operations thereby increasing the cost. In order to make flapping wing MAVs attractive in search, rescue, and recovery efforts, they should be disposable from the cost point of view. This can be achieved by 1) utilizing a scalable manufacturing process such as injection molding to amortize the part cost and 2) using innovative mechanism design methodology so as to reduce overall part count. This will lead to reduced assembly cost. The complex shape of the MAV mechanism will require us to design and develop new multi-piece mold designs to reduce the molding cost and the part count without compromising the structural integrity of the drive mechanism.

- ***High Power Transmission Efficiency***: In order for a flapping wing MAV to work, the rotary motion of the motor needs to be converted into flapping wing motions. Moreover, the motor speed needs to be reduced to match the desired wing flapping frequency. Power transmission from the motor to the wings is accomplished by the drive mechanism. The efficiency of the power transmission is a major concern. Due to weight considerations, low-friction bearings cannot be used in this application. Losing too much power in the transmission will reduce the operational range and also require use of a bigger motor. Hence, we are interested in exploring new concepts such as compliant drive mechanisms to minimize the power loss in the transmission without increasing the mechanism weight.

This paper describes an approach for determining the drive mechanism shape and size that meets both the design and molding requirements. The problem addressed in this paper has many facets that need to be simultaneously considered. The primary objective is to minimize the weight of the drive mechanism. The secondary objective is to select the structure shape to minimize the number of mold pieces. The structure shape and size need to ensure that the forces acting on the structure do not induce excessive stresses. Furthermore, structure shape and size need to respect molding constraints. Finally, the structure shape should be such that it is feasible to place weld-lines in low-stress area on the structure. In this paper, we describe a detailed approach for decomposing this challenging problem into more manageable steps. We also

demonstrate that the drive mechanism design generated by the approach described in this paper can be used to successfully realize a flapping wing MAV.

2 Overview of the Product and Process Design

In this section we list the main requirements for the drive mechanism, describe a mechanism concept, and describe the main steps in our approach for converting the concept into a detailed design.

To drive the mechanism we chose a DC pager motor as the source of the rotary motion, due to sufficient efficiency and acceptable weight. We then picked the lightest matching remote control receiver, tail actuator and battery cell. We empirically determined that the overall weight of the MAV had to be restricted to be 15 grams or less. Considering the weight of the electronics and the gearing that we had to use for the operation of the MAV, we determined that the weight of the mechanism had to be kept under 1.5 grams.

The primary functional requirement for the MAV drive-mechanism is that the flapping action of both wings should be synchronized. Based on the exploratory tests of the flying prototype, we determined the range of flapping to be 65°. Importance of synchronization is emphasized, because it not only ensures the required flapping action for a successful flight of the MAV, but also contributes to the overall stability of the mechanism. Our preliminary tests indicate that with the wing area of 2.6E-02 m^2, the flapping frequency will need to be at least 7 Hz to sustain flight.

The main functional requirements for the drive mechanism were as follows:

- Flap wings at more than 7 Hz
- Achieve flapping range between –12.5° and +52.5°
- Transmit motor torque of 6.6E-04 Nm
- Support wings of total area of 2.6E-02 m^2

Based on the weight, size, and functionality constraints, we determined that a compliant mechanism would be highly suitable for realizing the drive mechanism [9-11]. This is because a compliant mechanism minimizes losses due to friction and is easy to manufacture since it consolidates many parts into a single part. Figure 1 shows the schematic diagram of the mechanism concept. Flexural members were incorporated into the mechanism to provide for compliance in the structure to facilitate motion.

The constraint on the weight of the mechanism led us to choose a polymer as the material for the mechanism. We chose HIVAL ABS HG6 for manufacturing mechanism parts. Considering the choice of material, the small size scales involved, the shape complexity and the desire for a scalable manufacturing process, injection molding using multi-piece molds was selected to be the best choice for the manufacturing process for the mechanism [12-19]**.** Multi-piece molds have multiple mold opening directions. Designing multi-piece molds pose a significant design challenge due to increased mold cost, flash generation and demoldability of the part.

Moreover, the complexity of the part shape and small size scales make it necessary to use multi-gate molds. Placement of gates is a challenging problem since multi-gate molds lead to weld-lines on the structure [20-22]. Improper gate positioning may lead to a weld-line being positioned in a structurally demanding region of the part thereby leading to its failure.

The main decision variables for this problem are part shape, size, parting lines, gate locations, and sacrificial shape elements. The primary objective function for this problem is minimization of the weight. The secondary objective function for this problem is minimization of number of mold pieces. The following three constraints need to be satisfied. First, the stresses in the structure should not exceed the material limit. Second, the structure shape and size should meet molding process constraints. Finally, there should exist a feasible gate placement that ensures that the weld-lines are located in the low stress area of the structure.

We have decomposed this challenging problem into three main steps. The first step performs weight minimization of the structure while meeting stress constraints and dimensional constrains of the molding process. This step is described in Section 3. The design generated by this optimization is then optimized further during the second step by altering the shapes of non-critical features to minimize the number of mold pieces. This step needs to ensure that the constraints met during the first step are still satisfied. This step is described in Section 4. To ensure mold filling for a complex part

involving a multi piece mold, gate placement strategy needs to be examined in detail. The location of the gates directly influences warpage in the part as well as location of weld-lines. Section 5 describes an approach for placing gates and sacrificial elements to meet weld-line location constraints.

3 Mechanism Shape Synthesis

The first step in our overall approach is to determine the detailed part shape and dimensions from the concept illustrated in Fig. 1. Towards this end, we carried out the shape synthesis of the mechanism using the following three step approach. First, to generate a basic shape of the mechanism, we detailed the design concept by adding functionality and moldability constraints. Second, we determined the constrained dimension of the mechanism by analyzing mating components and motion requirements. Third, we utilized parametric optimization and Finite Element Analysis (FEA) to determine the values of other critical unconstrained dimensions. This approach is presented in Fig. 2 and discussed in further detail in this section.

3.1 Elaboration of Basic Shape

To obtain the flapping wing action from the rotary input of the motor we designed a crank-rocker mechanism based on the concept illustrated in Fig. 1. The motor's rotational velocity is transferred to the crank through a gearbox to adjust to the required flapping frequency. The crank is connected to a rocker, which displaces the symmetrically placed wing arms. These arms are mounted (pivoted) on the compliant members, which allow for the displacement of the pivoting point, hence feasible mechanism action. Note that this mechanism concept without the use of compliant members would be just a stationary structure.

We machined several prototype versions based on the design concept illustrated in Fig. 1 to asses the extent of disturbance forces and their effects. The experimental results showed that disturbance forces can cause significant out of plane motion of the gears and the wing supports. To eliminate these issues, we came up with a bi-planar design of the frame (Fig. 3). Introduction of this design allowed for two-point support for several elements in the mechanism. This also constrained the motion of the wing supports to lie in one plane. This was crucial to the amount of thrust produced by the wings of the MAV. The bi-planar design also protected the mechanism from impact loads during crash landings. The point exposed to the impact loads the most is the lowest point on the frame. Hence we designed the frame such that it provided an enclosure for the gear.

The issue of wobbling also affects the crank of the mechanism, which transmits the torque from the gear to the rocker. Due to significant forces acting on it, the two-point support of its rotation axis was a must. To reduce the friction and allow for easier assembly, we introduced a brass sleeve as the crank axis bearing.

In order to reduce the rotational velocity of the motor to match the flapping frequency requirement, we designed a two-step gear reduction of 26.66:1. This was the closest feasible matching combination of already available spur gears with module 0.3, chosen to be consistent with the size scale.

In order to ensure moldability of the mechanism gear-frame, we introduced fillets around the shafts' locations to minimize the differences of the cavity cross-section and allow for better melt flow in the mold. This is shown in Fig. 3.

After identifying the basic shape of the mechanism using the functionality and moldability constraints, the next step was to determine the dimensions of the mechanism. Considering the constraints on the overall size of the MAV, it was important to first identify the constrained and free dimensions of the mechanism body. We identified the constrained dimensions from the functional requirements of the MAV.

The design of the mechanism required the motor to be placed between the flexural members. Hence the size of the motor (7 mm in diameter) constrained the minimum separation between the flexural members to 16 mm. From these constraints we designed the overall length of the mechanism to be 41.7 mm. Figure 4 illustrates the fixed and free dimensions of the mechanism body based on the functional constraints described above. For the flapping range of 65° we designed a relative angle on the wing arms to be 15° and the length of the crank and the rocker to be 4 mm and 28 mm respectively. The key dimensions of our flapping wing drive mechanism are shown in Fig. 5.

Moldability constraints of the mechanism body required that the main parting direction of the mold had to be parallel to the z direction. Hence the minimum breadth b of the members was limited to 0.89 mm. This will be discussed in greater detail in the next section.

3.2 Estimation of Forces for Parametric Optimization

In order to perform structural analysis of the mechanism parts, we had to estimate the forces acting on them. One has to realize, that the mechanism in motion is a time dependant problem, but since the maximum wing flapping frequency based on the motor characteristic was 13.4 Hz and the masses of the moving elements were relatively small, we decided to neglect the inertial forces and performed static analysis for multiple time frames of the motion cycle. Due to the bi-planar design of the mechanism frame, the out-of-plane forces resulting from the motion were small. Therefore we simplified the kinematic modeling by treating it as a planar mechanism.

Due to the usage of compliance of members as a functional characteristic, we modeled the drive as pseudo-rigid body planar mechanism. The compliant members were modeled as rigid links with torsion springs at anchoring joints. The rotational stiffness of the spring was calculated according to Eq. (1). The sensitivity analysis showed that the influence of the rotational stiffness change on the sought reaction forces is very minor – change of k_{rot} by 10% changed the reaction forces only by less than 1%. A constant rotary motion Ω was applied on the motor shaft.

$$k_{rot} = 3\,E\,I\,/\,l \quad [\text{N m / rad}] \tag{1}$$

where:

k_{rot} – Rotational Stiffness

E – Young's Modulus

I – Moment of Inertia

l – Beam Length

The model kinematic representation along with the key dimensions is shown in Fig. 5. The force resulting from the wing action was modeled normal to the wing spar in the middle of its length, with a sign depending on upstroke/downstroke action. In order to estimate the maximum force applied to the wings, we used the value that resulted in the peak motor torque value equal to the stall torque for the motor. The manufacturer specified stall torque for the motor at 0.657 Nmm. The estimated force for this torque was 0.19 N. Weight of components did not contribute much to the reaction forces and hence it was ignored. After building a prototype we measured the lift force on the wings and the measured value was 0.15 N (see Section 6). Hence this estimate was a conservative approximation.

The key modeling inputs are listed in Table 1. The model synthesis is presented in Fig. 6**.**

We modeled the above mechanism in MSC Adams/View 2005 software and used it for the reaction force distribution analysis. We ran the static equilibrium simulation for two full wing flap cycles. Since this is a time-dependant problem, we had to find the cases where the combined load on the structure induced the highest von Mises stresses. In order to do so, we recorded and plotted the reaction forces at points A to E (Fig. 5) with the resolution of 10^{-4} sec. We divided the flap cycle into 20 load cases (every 18° of 360° of crank rotation). We also considered additional load cases with peak deflections of the compliant members and peak magnitudes of the loads. Finally, we recorded the sought components of forces acting on the mechanism frame at the picked time frames to obtain the inputs for the chosen combined load cases. This approach can be generalized to any time-dependant loading of designed part. Note that careful and rational choice of the combined loading cases will lead to reduction of finite element analyses described in the following subsection.

3.3 Parametric Optimization

After constraining the dimensional parameters of the mechanism to accommodate mechanical and electronic components required for the functionality of the MAV, we had to determine remaining critical unconstrained dimensions, namely b and t shown in Fig. 4. These were assigned by FEA-based design optimization.

The principle idea was to minimize the weight of the mechanism, yet the manufacturing and maximum allowable stresses constraints had to be satisfied. As mentioned before, the mold manufacturing constraint led us to set the width *b* of the compliant members to be 0.89 mm. This was due the tool path generation for machining the mold cavity. The remaining free dimension constrained by maximum allowable stresses was then minimized.

In order to reduce the number of FEA iterations, we picked six load cases at the final stage of wings' downstroke which, as expected, resulted in the maximum von Mises stresses along the structure. The forces applied in one of the cases are listed in Table 2. Since forces resulting from the weight of motor and gears were an order of magnitude smaller than the forces resulting from the motion, we did not include these forces in the FEA. We applied the estimated loads at points A to E (Fig. 5) to the corresponding points of the 3D frame model, as shown in Fig.7(a). These loads were applied at surface patches as indicated in Table 2. In addition, we applied a load corresponding to the drag force as negative of the measured peak thrust produced by MAV. This force was applied to the top of the front of compliant members (points A and B). We constrained the displacements of the frame structure where it is mounted to the MAV body – at the back surface of the motor holder and the back surface of the bottom extrusion connecting the frames. These surfaces are indicated in Fig. 7(a) as F and G, respectively. We assigned ABS properties (density=1040 kg/m^3, Poisson's ratio=0.3, Young's Modulus=2.3GPa) as the frame model material.

We performed the FEA of the six load cases and plotted maximum von Mises stresses along the structure. The yield strength of the material was divided by the maximum value of stresses observed by the part to obtain the resulting factor of safety. We designed the frame to have factor of safety of 1.75. This is average recommended value for known materials with certification under reasonably constant environmental conditions, subjected to loads and stresses that can be determined using qualified design procedures. Hence we solved for the depth *t* of the compliant members to be 1.52 mm.

We used Mechanica module of ProEngineer Wildfire 3.0 software to perform the FEA. The analysis ensured that the stresses resulting from the frame loads are safe and also identified the high stress and displacement regions shown in Fig.7(b). This is important for recognizing the areas which cannot contain weld-lines, and therefore useful for gate placement for molding. This will be discussed in further detail in Section 5.

Solving the design optimization problem as described in this section enabled us to get the complete set of dimensional parameters of the mechanism. The next challenge involved coming up with a detailed parting line design for molding the body-frame of the mechanism.

4 Mold Piece Design for Molding the Mechanism

The first step towards the mold design solution involved determination of the appropriate parting lines and thereby the total number of mold pieces required for molding the mechanism body. The complexity of the shape of the body-frame made the mold piece design a challenging problem. To address this problem in a systematic manner, we modified and adopted the approach outlined by Priyadarshi and Gupta [13]. The following four steps are used in our approach:

1) A candidate parting direction set *D* is found in two steps. In the first step, an initial set of heuristic directions *D* is found. If there are facets that are not accessible from any of the directions in *D*, additional directions are found and inserted into *D* in the second step. To generate mold-pieces, directions from which most of the faces are accessible, are required. It is observed that the following directions are usually good candidates for a parting direction (1) Planar Face Normal and (2) Cylindrical/Conical Face Axis. A candidate parting direction set *D* is determined by finding the above two types of directions. Please note that the planar face normals and cylindrical/conical face axis are found using the boundary representation. For each direction *d* in *D*, *-d* is also included in *D* because a two-piece mold may exist with the parting direction *d*. After computing the initial set *D*, we facet the parts into small facets and perform accessibility analysis using directs in *D*. There may still be some facets that are not accessible from any of the directions in *D*. Exact accessibility analysis is performed for each such facet to check whether it is accessible from any direction at all. If upon performing the accessibility analysis (see Dhaliwal et al. [23]) any direction is found, that direction is inserted into *D*. Otherwise the part is rejected as non-moldable.

2) For each direction *d* in *D,* we find the set of facets that are accessible from direction *d*. The set *V* represents accessible-facet sets. Each member of *V* corresponds to a direction in *D*. Using the set *V* of accessible-facet sets, the part boundary is then divided into different regions called mold-piece regions. A mold-piece region is a connected set of facets that can be formed by a single mold piece. This step is performed using graph search on the adjacency graph of every accessible-facet set. We use set *G* to represent mold piece regions.

3) Out of all mold-piece regions, minimum number of mold-piece regions is selected such that the entire part boundary is covered. This is equivalent to solving set-cover problem. We first analyze set D to identify the required parting direction. In our approach we always consider the direction perpendicular to the plane that maximizes the part projection as the required parting direction. Two sets from V that correspond to this pair of parting directions are always added to the solution. The remaining mold piece regions are identified using breadth-first search.

4) The boundary of a mold-piece region is a valid parting line, but it may not be a good parting line. A good parting line is characterized by simple mold pieces that are inexpensive to operate and manufacture. A mold-piece region $r = (d, F)$ contains two types of facets: *primary facets* and *secondary facets*. Primary facets are present only in r, i.e. they cannot be formed by the mold piece of some other mold-piece region. Secondary facets are also present in other mold-piece regions, i.e. they can also be formed by the mold pieces of other mold-piece regions. Hence some common facets may be excluded from r to improve the quality of the parting line. A belt of common facets is determined by growing the boundary of the mold-piece region inwards. This belt provides a feasible region E where an optimal parting line can be located. The flatness criteria proposed by Majhi et al. [24] is then used to find the flattest possible parting line.

A part may have non-critical shape elements (e.g., connectors on a mechanism). Changing the shape of these connectors could potentially have the desirable effect on reducing the number of mold pieces required for demolding of the part. Hence the shape or geometry resulting in minimum number of mold pieces is selected for such non-critical connectors. Changing the connector shape necessitates repeating the FEA to confirm that the stress levels in the part were acceptable. If they are unacceptable, the feature dimensions have to be modified to satisfy the stress constraints. Once the final shape of the part is optimized to obtain the minimum number of mold pieces, the next step is to include demoldability and flash considerations in the mold design. In a multi-piece mold, to ensure demoldability of the part, the molded part should stick to only one mold piece during mold piece separation. This is ensured by having higher number of part facets in one mold piece region. If this is not the case, then sacrificial shape elements need to be added to the appropriate mold piece region so as to increase the total number of part facets in this mold piece region. Sacrificial shape elements are also needed to absorb flash in non-critical areas. These sacrificial shape elements are added in such a way that the existing parting directions for the molded part remain constant.

For the body frame that we have considered in this paper, the design obtained after incorporating the constraints of the functional requirements and performing the mechanics-based optimization consisted of a non-critical shape element for the motor support. We considered three different regular polygonal (e.g., triangle, square, and hexagon) and circular shapes for this element. The radius of the maximum circle contained in each shape was kept the same. Two different orientations were tried for each polygon. The first orientation involved a polygon edge aligned with the x-axis. The second orientation was derived by rotating the triangle by 60 degrees, the square by 45 degrees, and the hexagon by 30 degrees. For each shape, we determined the total number of mold pieces required for molding the part using the steps outlined above. From this method, we established the shape of the motor support for minimum number of mold pieces to be an inverted triangle (Fig. 8).

The mold design after optimizing non-critical shape elements consisted of 5 mold pieces and 5 mold side cores. The mold pieces that constituted the mold assembly are shown in Fig. 9. The demolding process for the part using this mold design is illustrated in Fig. 10. After mold piece design, we had to check the design for part demoldability and flash. To ensure demoldability, we had to add a sacrificial shape element to the top mold piece illustrated in Fig. 9. Addition of an appropriate size of this sacrificial shape element ensured that the overall part volume was appropriate to avoid flash and overcome under-filling of the part. After mold piece design, the next step involves placement of gates.

5 Gate Placement

After a feasible parting surface design is identified, the next issue that needs to be addressed is the gate placement. Gate placement strategy is one of the most important mold design decisions that need to be made. The location of the gates on the part affects several important parameters, which are 1) mold cavity filling, 2) warpage in the injection molded part and 3) location of weld-lines.

The first step to determine the position of the gates was to identify the feasible areas on the part where the gate could be located. Location of gates on features that would be subjected to high stress levels during operation lead to stress concentrations. High stress areas are classified as:

1) Functional stresses: Stresses appearing on the part during its regular operation

2) Demolding stresses: Stresses occurring during demolding of the part from the mold cavity

Hence, placement of gates in these locations is highly undesirable, since this would result in even higher stress levels in these areas. Therefore the feasible areas for gate locations should be identified as regions, which are not subject to high stress levels. Once the feasible areas for the gate locations are identified, the next step involves determining the number of gates required to ensure appropriate part filling with acceptable levels of warpage. In this step, the gates can be initially placed symmetrically within the part region containing the allowable gate locations. Filling simulations in Moldflow Plastics Insight 6.1 reveal the effect of the gates on the part filling. However, the gate positions identified for appropriate mold filling may not ensure appropriate positions of weld-lines in the part. Hence, the next step involves positioning the gates such that the weld-line locations are acceptable. Weld-lines should not be located at areas which could potentially be exposed to high stresses.

Therefore the gates needed to be moved to more appropriate regions to ensure proper weld-line locations. However, some situations may necessitate addition of a gate to alter weld-line locations. While moving or adding the gates, it is important to ensure that the part filling is not adversely affected by the new gate positioning. Addition or repositioning of gates may not be sufficient to eliminate all the weld-lines that result from part molding. Hence, sacrificial shape element may have to be added, to absorb weld-lines occurring in other critical areas. The overall approach used for gate positioning and sacrificial shape element design to absorb weld-lines is outlined in Fig. 11. Using this approach, we solved the gate positioning problem for the body-frame.

As the first step, we determined the allowable area for gate locations to be only along the gear-frame, as illustrated in Fig. 12.

To identify the gate locations for appropriate mold filling and optimum location of the weld-lines, we initially placed one gate on the gear-frame in a region shown in Fig. 12**.** We then ran filling simulations to determine the fill time, the bulk temperature at the end of the fill and the location of the weld-lines. For the filling simulations, we used ABS as the material. The process simulation settings used are listed in Table 3.

The result of the flow simulation for a single-gated mold showed a large variability in the fill time of the polymer in different parts of the cavity. This resulted in a highly asymmetric filling of the cavity. This asymmetry in filling could potentially lead to a high degree of warpage. We obtained the warpage present in a part fabricated using a single gated mold. The measured value was found to be 6.9°. A single-gated mold was therefore inappropriate for manufacturing functional gear-frames. The results of the filling simulations elucidate the advantage of using a double-gated mold and the corresponding symmetry obtained in the filling of the part.

In the next step, we isolated the high stress areas on the molded body-frame. These positions were obtained from the FE simulations conducted earlier as illustrated in Fig. 7. These positions were therefore unacceptable weld-line locations.

The weld-lines form wherever polymer melt has to flow around a side mold core. We have used side mold cores to obtain cylindrical holes in the structure. These holes were critical for the assembly of the body-frame to other components of the mechanism of the MAV. In a two gate mold a weld-line was formed on the structure which joins the two planes of the body-frame near the bottom. Since the strength of this structure is considered as critical, the weld-line in this position is highly undesirable. Hence it was necessary to either eliminate this weld-line or move it to non-critical area of the body-frame. While moving the weld-lines care has to be taken that they are not moved to high stress areas of the part.

Repositioning the gates was undesirable since this resulted in asymmetric mold filling. Hence, to move this weld-line to a more desirable location, we had to add an extra gate to the mold. We placed this gate such that there would be 1) even melt flow to different parts of the cavity resulting in complete mold filling, 2) lower temperature gradients of the melt in different parts of the mold cavity resulting in lower warpage, and 3) weld-lines will appear at acceptable locations.

This gate moved the weld-line to the area of the gear-frame which was exposed to significantly lower demolding stresses. This is illustrated in Fig. 13.

However, weld-lines were still present in undesirable locations as illustrated in Fig. 13. Placement of additional gates would be unable to overcome this problem. Hence, we had to design sacrificial shape elements to eliminate these weld-lines.

To absorb the undesirable weld-lines illustrated in Fig. 13, we added sacrificial element 1 as shown in Fig. 14. This element was strategically placed near the top of the flexural members between the top and bottom mold pieces. This element completely eliminated weld-line originally forming on the top of the flexural members. Secondly, it provided a connection between the top and bottom mold pieces ensuring a better melt flow between the cavities. Finally, it ensured that the molded component stuck entirely to the middle layer while demolding, resolving problems with part ejection.

The second sacrificial element was added to the gear-frame. This element was added solely to ensure that the molded part sticks to one half of the mold. This was outlined in the Section 4. The location of the weld-lines in the molded part which contains the sacrificial elements is illustrated in Fig. 14.

Introduction of additional gates and sacrificial elements resulted in improvement of the mold part quality. It also enabled ease in demolding. The final gate configuration and the location of the sacrificial elements are illustrated in Fig. 15.

6 Results and Discussions

We molded the parts of the drive mechanism on a Milacron Babyplast injection molding machine. We used HIVAL ABS HG6 for manufacturing the parts of the mechanism.

Figure 16 shows the photograph of the part that was molded using the molding strategy discussed in this paper. Careful visual inspection of the part revealed that the weld-line was present at the predicted location, illustrated in Fig. 15. As can be seen in the side view of the molded part in Fig. 16, some warpage (about 1.28°) is still present in the molded structure. From this it can be concluded that the differential shrinkage of the part could not be completely eliminated. Nevertheless, since it did not affect the functionality of the mechanism, we concluded that the warpage in the structure was functionally acceptable.

After successfully accomplishing the molding of the body-frame, we also molded the rocker and wing supports of the mechanism.

Finally, we assembled the MAV using the molded parts along with the gears and the electronics. The MAV that was designed and developed in the Advanced Manufacturing Laboratory is illustrated in Fig. 17. The MAV was hand-launched and was capable of holding a sustained flight with controlled ascent and descent. We were also able to successfully steer and land the MAV indoors. The main performance specifications are listed in Table 4. Video of the successful flight can be found at http://terpconnect.umd.edu/~skgupta/UMdBird/

We used a linear test stand with 1-DOF to measure the thrust and lift of the MAV. The robot was mounted in a clamp fixed to the low-friction rigid linear air bearing RAB1S from Nelson Air. Within the cavity of the bar held by the bearing, a COOPER LFS270 load cell was mounted to measure the load occurring due to thrust force while the mechanism is running. The resolution of the load cell is 0.025 g. In reaction to the applied thrust force, the COOPER Instruments Bridge Amplifier DCM465 transformed the voltage of the load cell into a digital signal. The National Instruments' Measurement & Automation Explorer software was used to record the voltage over the time. Then the voltage was converted into a weight load with the load cell calibration factor. The measured average thrust was 0.077 N and peak thrust was 0.0981 N when the MAV was attached to a stationary platform. We then repeated the experiment with the robot fixed vertically to measure the average lift. The measured peak lift value was 0.15 N when the MAV was attached to a stationary platform.

We compared the performance of the drive mechanism of our MAV with a commercially available iFly [25]. The drive mechanism of our MAV was 33% lighter than that on iFly. Moreover our drive-mechanism was capable of transmitting over 2 times the torque of iFly. Our drive mechanism provides 65° range of motion compared to 45° by iFly.

7 Conclusions

This paper describes an approach for determining the drive mechanism shape and size that meets both the design and molding requirements. The novel aspects of this work include (1) reorienting non-critical shape features to minimize the number of mold pieces and (2) the use of sacrificial shape elements to reduce the impact of the weld-lines on the structural performance.

The method described in this paper is applicable to any complex structural load bearing member that needs to be manufactured using multi-piece multi-gate injection molds. We have described an integrated approach for the part design by taking into account 1) the structural and functional requirements of the design and 2) the moldability requirements of the part. The following new results are reported in this paper. First, we present an integrated shape synthesis

methodology for developing a concept under functionality and moldability constraints. Second, we describe a method to select shape features to minimize the number of mold pieces required for molding a part. Next, we describe the use of innovative cavity gating methods to move weld-lines in the part to structurally less demanding portions. Finally, we describe an approach to design sacrificial shape elements which absorb weld-lines previously present on critical features. The sacrificial elements also provided the advantage of assisting demolding of the part.

We have successfully met the three requirements described in first section. Our design framework allowed us to minimize weight and give us payload capacity of 2.5 g. The use of compliant mechanism reduced the number of rigid body joints and hence reduced power loss in the transmission. It also led to significant reduction in part count. This can potentially lower the assembly cost of the drive mechanism. The use of injection molded drive mechanism is also expected to reduce the cost of the drive mechanism. We have successfully demonstrated technical feasibility of using the injection molding process for fabrication of the flapping wing drive mechanism. Using injection molding, which is a low cycle time and high throughput process, results in significant reduction of production cost. We have shown that the mold design described in this paper enables (1) successful demolding of the part, (2) elimination of excessive flash generation, (3) acceptable level of warping, and (4) elimination of weld-lines from high stress areas. Using this multi-piece, multi-gate mold design led to significant reduction of the part count. This directly resulted in low overall weight of the part used as a drive-mechanism for a bio-inspired MAV. We have demonstrated successful flight and steering capabilities of this MAV.

8 Acknowledgements

This research has been supported by the Army Research Office through MAV MURI Program (Grant Number ARMY W911NF0410176) and NSF grants DMI-0457058 and OCI-0636164. Opinions expressed in this paper are those of the authors and do not necessarily reflect opinions of the sponsors.

9 References

[1] Madangopal, R., Khan, Z.A., and Agrawal, S.K., 2005, "Biologically Inspired Design of Small Flapping Wing Air Vehicles Using Four-Bar Mechanisms and Quasi-Steady Aerodynamics,". J. Mech. Design, **127**, pp. 809-816.

[2] Madangopal, R., Khan, Z.A., and Agrawal, S.K., 2006, "Energetics-Based Design of Small Flapping-Wing Micro Air Vehicles," IEEE/ASME Transactions on Mechatronics, **11**, No.4.

[3] Galinski, C., and Zbikowski, R., 2007, "Materials Challenges in the Design of an Insect-Like Flapping Wing Mechanism Based on a Four-Bar Linkage," Materials & Design, **28**, No.3, pp. 783-796.

[4] Cox, A., Monopoli, D., Cveticanin, D., Goldfarb, M., and Garcia, E., 2002, "The Development of Elastodynamic Components for Piezoelectrically Actuated Flapping Micro-Air Vehicles," J. Intelligent Material Systems and Structures, **13**, No.9, pp. 611-615.

[5] Banala, S.K., and Agrawal, S.K., 2005, "Design and Optimization of a Mechanism for Out-of-Plane Insect Winglike Motion with Twist," J. Mech. Design, **127**, No.4, pp. 841-844.

[6] Conn, A.T., Burgess, S.C., and Ling, C.S., 2007, "Design of a Parallel Crank-Rocker Flapping Mechanism for Insect-Inspired Micro Air Vehicles," Proceedings of the Institution of Mechanical Engineers Part C - J. Mechanical Engineering Science, **221**, No.10, pp. 1211-1222.

[7] Tantanawat, T., and Kota, S., 2007, "Design of Compliant Mechanisms in Minimizing Input Power in Dynamic Applications," J. Mech. Design, **129**, No.10, pp. 1064-1075.

[8] Zdunich, P., Bilyk, D., MacMaster, M., Loewen, D., DeLaurier, J., Kornbluh, R., Low, T., Stanford, S., and Holeman, D., 2007, "Development and Testing of the Mentor Flapping-Wing Micro Air Vehicle," J. Aircraft, **44**, No.5, pp. 1701-1711.

[9] Mankame, N.D., and Ananthasuresh, G.K., 2004, "A Novel Compliant Mechanism for Converting Reciprocating Translation into Enclosing Curved Paths," J. Mech. Design, **126**, No.4, pp. 667-672.

[10] Zhou, H., and Ting, K., 2006, "Shape and Size Synthesis of Compliant Mechanisms Using Wide Curve Theory," J. Mech. Design, **28**, pp.551-558.

[11] Howell, L.L., 2001, "Compliant Mechanisms," Wiley-Interscience.

[12] Beaumont, J.P., 2004, "Runner and Gating Design Handbook: Tools for Successful Injection Molding," Hanser Gardner Publications.

[13] Priyadarshi, A., and Gupta, S.K., 2004, "Geometric Algorithms for Automated Design of Multi-Piece Permanent Molds," Computer Aided Design, **36**, No.3, pp. 241-260.

[14] Beaumont, J.P., Nagel, R., and Sherman, R., 2002, "Successful Injection Molding: Process, Design, and Simulation," Hanser Gardner Publications.

[15] Kazmer, D.O., 2007, "Injection Mold Design Engineering," Hanser Gardner Publications.

[16] Madou, M.J., 2002, "Fundamentals of Microfabrication," CRC Press.

[17] Malloy, R.A., 1994, "Part Design for Injection Molding," Hanser Gardner Publications.

[18] Menges, G., Michaeli, W., and Mohren, P., 2001, "How to Make Injection Molds," Hanser Gardner Publications.

[19] Fuh, J.Y.H., Zhang, Y.F., Nee, A.Y.C., and Fu, M.W., 2004, "Computer-aided Injection Mold Design and Manufacture (Plastic Engineering)," CRC Press.

[20] Mathur, R., Fink, B.K., and Advani, S.G., 1999, "Use of Genetic Algorithms to Optimize Gate and Vent Locations for the Resin Transfer Molding Process," Polymer Composites, **20**, No.2, pp. 167-178.

[21] Shoemaker, J., 2005, "Moldflow Design Guide: A Resource for Plastics Engineers," Hanser Publishers.

[22] Henz, B.J., Mohan, R.V., and Shires, D.R., 2007, "A Hybrid Global-Local Approach for Optimization of Injection Gate Locations in Liquid Composite Molding Process Simulations," Composites: Part A, **38**, pp. 1932-1946.

[23] Dhaliwal, S., Gupta, S.K., and Huang, J., "Computing Exact Global Accessibility Cones for Polyhedral Objects," In ASME Design for Manufacturing Conference, Baltimore, MD.

[24] Majhi, J., Gupta, P., and Janardan, R., 1999, "Computing a Flattest, Undercut-Free Parting Line for a Convex Polyhedron, with Application to Mold Design," Computational Geometry Theory and Applications, **13**, pp. 229-252.

[25] iFly Vamp, 2008, Copyright Interactive Toy Concepts Inc.

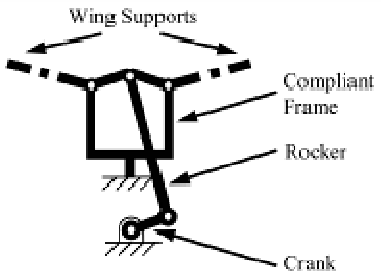

Fig. 1 Schematic diagram of compliant mechanism for flapping wing action

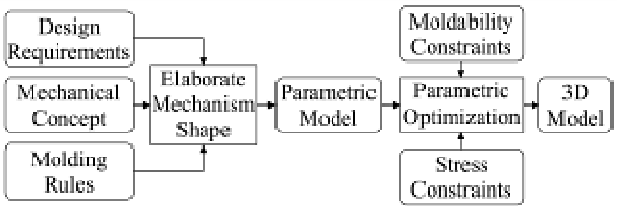

Fig. 2 Shape synthesis from the mechanism concept

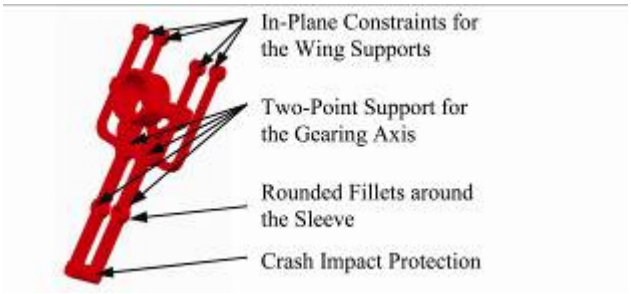

Fig. 3 Bi-planar design of the drive mechanism frame

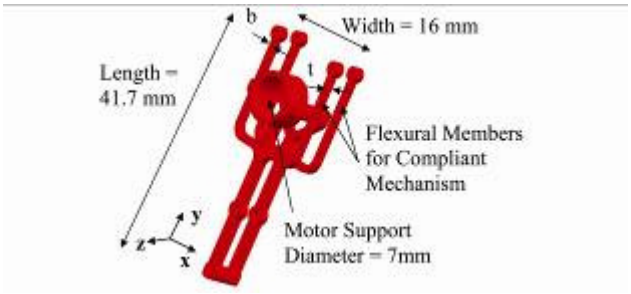

Fig. 4 Fixed and free dimensions of the mechanism body

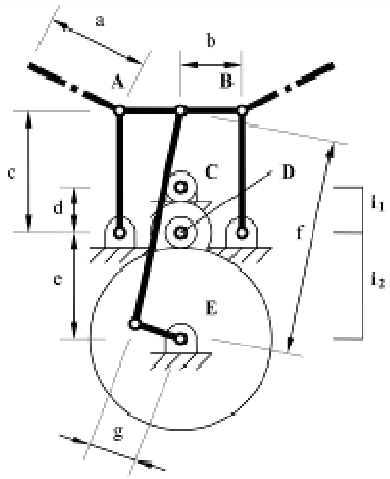

Dimensions:		
a	76	mm
b	8	mm
c	17.5	mm
d	8..5	mm
e	10.8	mm
f	28	mm
g	4	mm

Gear Reductions:		
i_1	**0.1875**	–
i_2	**0.20**	–

Fig. 5 Kinematic representation of the model

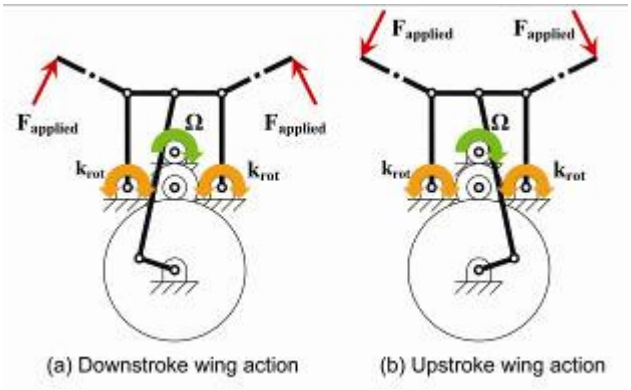

Fig. 6 Model synthesis

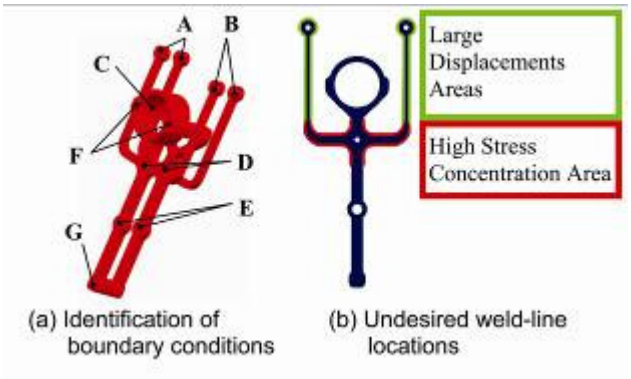

Fig. 7 FEA model and results

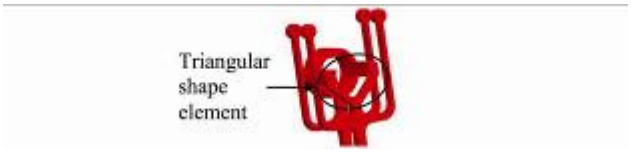

Fig. 8 Optimization of non-critical shape elements

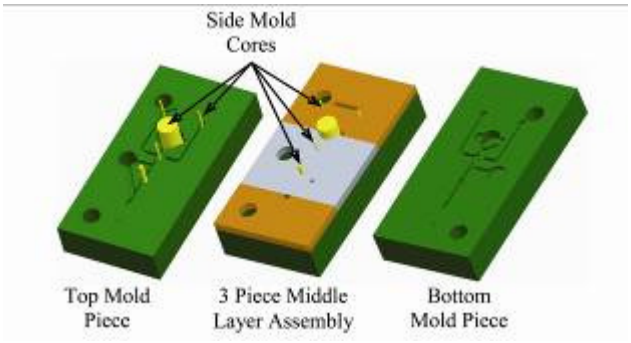

Fig. 9 5-piece mold design for body-frame fabrication

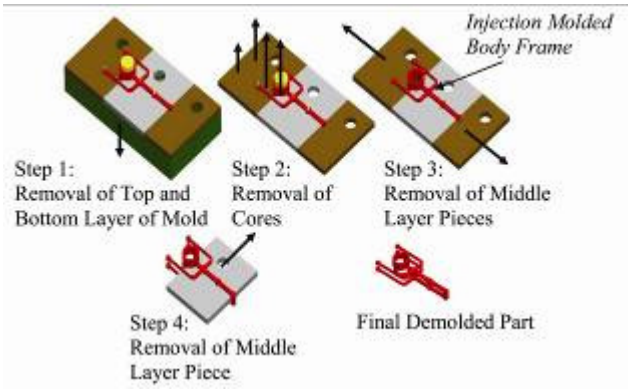

Fig. 10 Parting surface design for in-mold fabrication of the body-frame

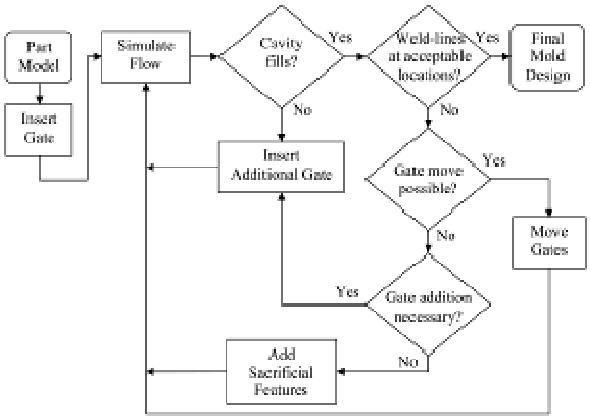

Fig. 11 Gate placement

Fig. 12 Allowable gate locations in molded mechanism frame

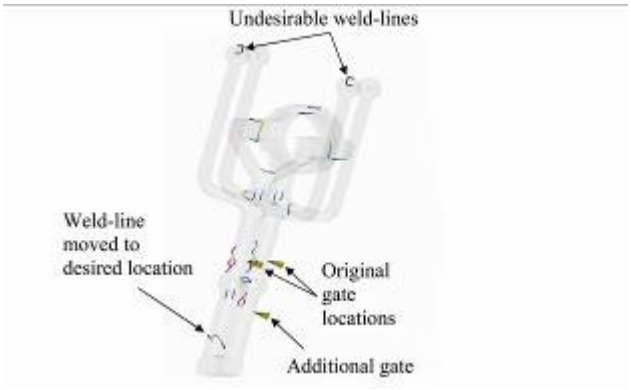

Fig. 13 Weld-line locations for three gated mold

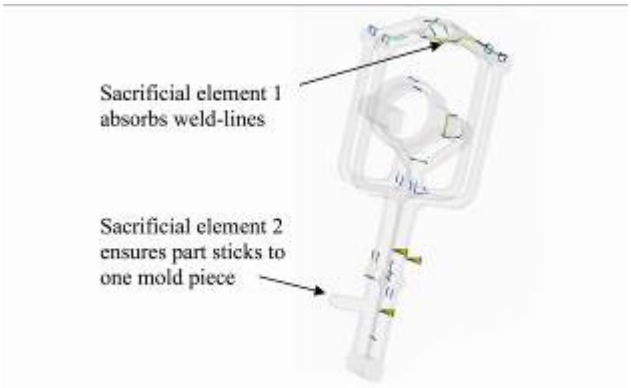

Fig. 14 Weld-line locations for three gated mold with sacrificial elements

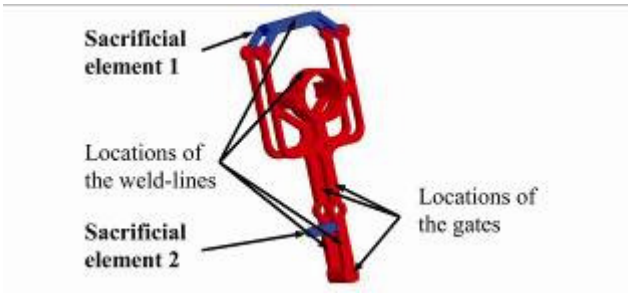

Fig. 15 Sacrificial elements for absorbing weld-lines

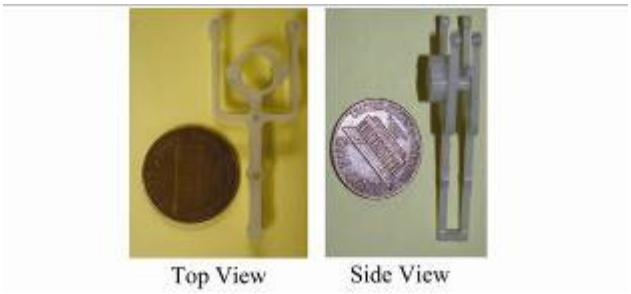

Fig. 16 In-mold fabricated body-frame

Fig. 17 Assembled MAV containing in-mold fabricated mechanism

Table 1 Modeling inputs

Torsion spring stiffness	k_{rot}	0.7	*N-mm/deg*
Motion applied	Ω	21387	*rpm*
Wing force resulting from flapping action	$F_{applied}$	0.19	*N*

Table 2 Components of applied forces in Newton for FEM case

Force	Applied to	X	Y	Z
CML_ARM	A	0.0809	2.6965	0
CMR_ARM	B	-0.4909	2.9448	0
PIN1	C	-0.2693	0	0
PIN2	D	1.3463	0	0
CR	E	-0.665	-5.2709	0
DRAG	A, B	0	0	0.0981

Table 3 Process settings used in flow simulation

Parameter	Value
Injection material	ABS
Injection temperature	240 C
Mold temperature	25 C
Injection velocity	12 cc/s
Injection time	3 s

Table 4 Performance attributes of the MAV

Overall Weight	12.76 g
Payload Capability	2.5 g
Maximum Flapping Frequency	12.1 Hz
Flight Duration	5 min
Flight Velocity	4.4 m/s